

Gas phase thermometry of hot turbulent jets using laser induced phosphorescence

Martin Lawrence, Hua Zhao, and Lionel Ganippa^{*}

Department of Mechanical Engineering

Brunel University,

Uxbridge, Middlesex,

UB8 3PH, UK

**lionel.ganippa@brunel.ac.uk*

Abstract: The temperature distributions of heated turbulent jets of air were determined using two dimensional (planar) laser induced phosphorescence. The jets were heated to specific temperature increments, ranging from 300 – 850 K and several Reynolds numbers were investigated at each temperature. The spectral ratio technique was used in conjunction with thermographic phosphors BAM and YAG:Dy, individually. Single shot and time averaged results are presented as two dimensional stacked images of turbulent jets. YAG:Dy did not produce a high enough signal for single shot measurements. The results allowed for a direct comparison between BAM and YAG:Dy, revealing that BAM is more suitable for relatively lower temperature, fast and turbulent regimes and that YAG:Dy is more suited to relatively higher temperature, steady flow situations.

1. Introduction

Temperature measurement techniques are used throughout a wide variety of applications from physical, to chemical and in biological processes. Laser thermometry enables in situ measurements to be carried out with minimal disturbances and with high spatial and temporal resolution, which is an advantage when measuring dynamic systems such as those in fluid flow and combustion. Improving the understanding of such systems will lead to more efficient real world solutions such as better engine designs, enhanced gas turbine aerodynamics and cleaner combustion.

Laser induced phosphorescence (LIP) is a semi-invasive, thermometry technique that uses the temperature dependent properties of thermographic phosphors (TPs) to determine the temperature of a system. A phosphor is a microcrystalline solid luminescent material and they are usually white in appearance. Phosphors are thermographic if they display variations in their emission characteristics with a change in temperature. TPs are generally made up of ceramic materials doped in rare earth metals [1]. Each chemical exhibits different absorption and emission characteristics, with varying temperature sensitivity and survivability capabilities, making TPs suitable for thermometry measurements in environments from cryogenic to combustion temperatures [2].

Phosphorescence is defined as long lived luminescence which can be explained by the radiative emission from a substance when transferring energy from an excited state to a lower energy

state. Phosphorescence differs from fluorescence as fluorescence occurs from electric dipole allowed transitions and phosphorescence occurs from forbidden ones [3]. TPs can have their lifetimes ranging from milliseconds to less than 1 nanosecond, making them suitable for measuring temperature in almost any situation [4].

Both the phosphorescence emission spectra and decay lifetime are affected by temperature variation [5]. Therefore it is possible to perform temperature measurements using two methods. The spectral method takes the ratio of two or more bands of the emission spectrum, compared with previously recorded calibration data, to convey the local temperature [6]. The temporal method records the time it takes for the phosphorescent emission to decay to a negligible amount [7], where a negligible amount is considered to be where the phosphorescence signal reaches a value similar to that of the background level. The time constant of the decay rate is usually determined by fitting a mono-exponential curve to the data, through which the temperature can be found when compared with a calibration measurement. Both methods can be used for either point [8] or planar measurements [9], achieved by using a focused laser beam or laser sheet, respectively. Planar measurements are essential for surveying a flow field and are advantageous for combustion studies.

The LIP technique has been applied to surface temperature measurements, such as thermal barrier coatings [10], optical access internal combustion engines [11] and gas turbine studies [12–14]. In order to carry out surface temperature measurements the TPs have to be adhered to the surface in question. Specific adhesives are required for this, which are called binder materials, this is usually a liquid which can be easily mixed with the TP powder and then the mixture painted onto the surface. Surface measurements are well established and the work has been reviewed in the following review articles [2, 4, 15]. More recently thermometry techniques using TPs have advanced from surface measurement to droplet and spray applications [16–18], where instead of the TP powder being attached to a surface it is suspended within a droplet of solution. This led the way for non-surface measurements, leading to the capability of gas phase temperature measurement, where TPs are seeded within the flow in powder form. Examples of previous studies in the gas phase include fundamental studies of heated jet temperature distributions [19–23] and practical applications of in-cylinder temperature measurements in engines [19, 24, 25].

LIP is a relatively simple technique with respect to the experimental setup and post processing methodology, compared to other laser-based thermometry techniques, such as CARS, LIF, LIGS and TLA. The limitations in terms of speed and temperature of the technique depend on the specific TP and therefore LIP could be applied to a wide range of surface and flow situations. TPs provide a high signal yield, where the intensity ratio is insensitive to oxygen quenching and is very negligibly affected by laser profile and TP concentration. Challenges that occur when using thermographic phosphors include overcoming the stickiness of the particles and discovering an efficient seeding method. The particles must be seeded within the flow with a sufficient enough volume density that a significant phosphorescence signal can be detected. Low signal to noise ratio is

one of the major concerns in gas phase LIP. These challenges are discussed in more detail later on in this paper.

This study focuses on using the spectral ratio method in conjunction with YAG:Dy and BAM to produce gas phase planar temperature measurements of heated turbulent jets issuing into quiescent air. Spectroscopic analyses of both phosphors were carried out in order to reveal the temperature dependence of the phosphorescence signal. Calibrations of both phosphors were carried out identically to the turbulent heated jet measurements. The LIP technique was applied to heated gaseous jets, producing both averaged and single shot data for the YAG:Dy and BAM phosphors. Temperature distributions were calculated using the data in conjunction with the calibrations and they are presented from 300 – 850 K at different flow conditions. Finally, precision and uncertainty evaluations are also discussed.

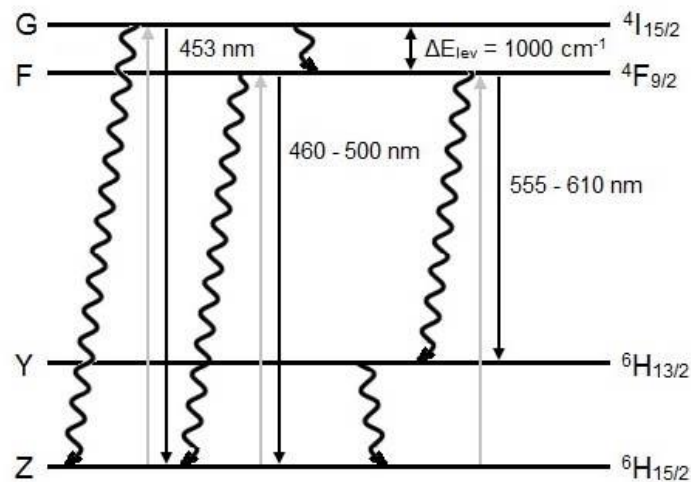


Figure 1. Simplified YAG:Dy³⁺ energy diagram, where grey arrows represent absorption of a photon and excitation to a higher energy level, black wiggly arrows represent non-radiative de-excitation mechanisms (phonons) and black straight arrows represent radiative de-excitation mechanisms (photons) i.e. phosphorescence.

2. Thermographic phosphors

2.1 YAG:Dy

YAG is the common name for yttrium aluminum garnet, with chemical formula Y₃Al₅O₁₂. The specific TP used in this study is Y₃Al₅O₁₂:Dy, which is YAG doped in trivalent dysprosium (Dy³⁺) ions. In this work 2.5 and 10.2 μm median diameter YAG:Dy particles (QMK66/UF-X and QMK66/N-X respectively) were used, which were provided by Phosphor Technology Ltd. YAG crystals are widely used in solid state lasers, such as Neodymium doped YAG (Nd:YAG) lasers. The

YAG:Dy crystal structure is described as body centered cubic, with Dy³⁺ ions replacing Y³⁺ ions at the dodecahedral Y³⁺ sites in the Y₃Al₅O₁₂ host lattice [26]. There are three emission bands in Dysprosium that occur from ⁴I to ⁶H transitions in the Dy³⁺ ion, see Figure 1 for details. The most energetic of which is an electric dipole around 453 nm, due to the transition from ⁴I_{15/2} to ⁶H_{15/2}. This band is weak near room temperature, but intensifies significantly as temperature increases [27]. The remaining blue part of the spectrum between 460 and 500 nm is due to electronic transitions ⁴F_{9/2} to ⁶H_{15/2}, corresponding to a magnetic dipole transition which is insensitive to crystal field symmetry around the Dy³⁺ ion. The yellow emission band from 555 - 610 nm is due to electronic transitions ⁴F_{9/2} to ⁶H_{13/2}, relating to a forced electric dipole transition which is strongly influenced by the surrounding environment. At a local site without inversion symmetry, the yellow emission is dominant, however for YAG:Dy³⁺ there is inversion symmetry and the blue emission is prevalent [26, 28].

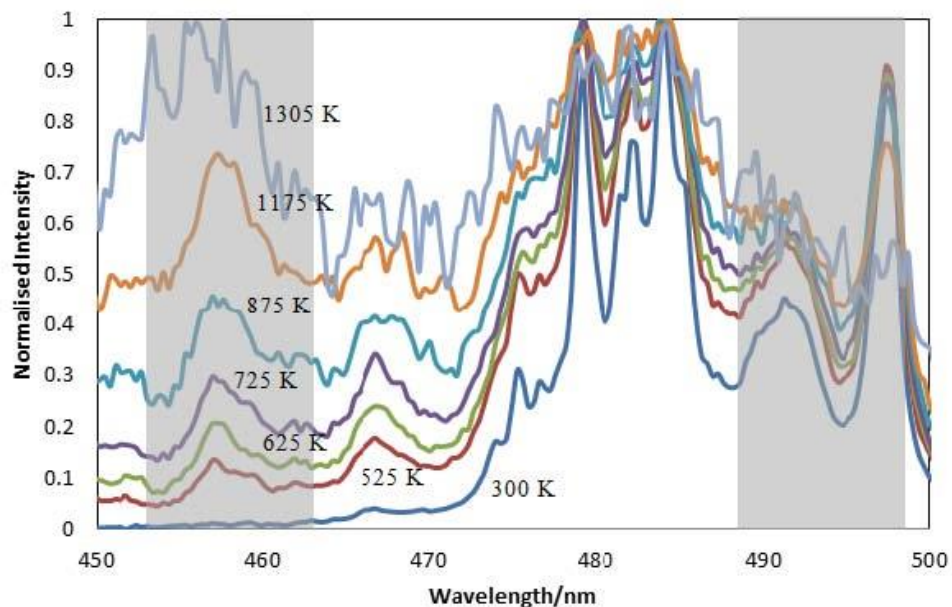


Figure 2. Normalized intensity YAG:Dy emission spectra at specified temperatures after 355 nm excitation, determined by surface measurements on a thermocouple coated in YAG:Dy using a high temperature binder, measured in the same position as the jet temperature measurements. The thermocouple was heated in two ways; in the hot air where temperature was varied by varying jet temperature and in a flame where temperature was measured by moving the thermocouple around the flame. The grey areas represent filters placed over the image doubler centered at 458 nm with a FWHM of 10 nm and centered at 492 nm with a FWHM of 10 nm.

Increasing the temperature can affect the spectrum of rare earth ions in several ways. Broadening of linewidth due to lattice vibrations, or phonons, which also reduce the radiative

transition lifetime via quenching, vibrational relaxation and internal conversions, represented in Figure 1 as wiggly arrows, where the increased vibration non-radiatively relaxes the excited electronic state. Thermal expansion of the lattice creates larger ion separation, which can lead to a frequency shift, reducing the crystal field and reducing Stark component separation [29]. An increase in the population of upper energy levels of the system, according to Boltzmann's law, causes the intensity distribution of the spectrum to change with temperature. This thermalization effect occurs when two rare earth energy levels are relatively close to one another. It can be seen from Figure 1 that YAG:Dy displays this in its F and G energy levels, which are separated by about 1000 cm^{-1} . Laser light can excite the Dy^{3+} ions into the F level, which undergoes fast thermal equilibrium and can pump some of its population to the G level and phosphorescence can then be observed from both states. At low temperatures, the G level will generally not emit phosphorescence due to very high multiphonon relaxation rates which quench the closely spaced levels. The population of the G level emission band rises with temperature, significantly increasing the amount of phosphorescence from this level. Above 1800 K the phosphorescence intensity reduces below detectable limits due to large phonon quenching rates at such high temperatures [29].

The melting point of the YAG crystal is approximately 2200 K [30]. Phosphorescence decay time ranges from 1 ms at room temperature to an order of 1 μs at high temperatures [27]. The survivability of the YAG:Dy phosphorescence has been investigated, where the intensity ratio was found to be the same before and after the phosphor particles had passed through a flame front [31].

2.2 BAM

BAM is the common name for barium magnesium aluminate, with chemical formula $\text{BaMgAl}_{10}\text{O}_{17}$. The specific TP used in this study is $\text{BaMgAl}_{10}\text{O}_{17}:\text{Eu}$, which is BAM doped in divalent europium (Eu^{2+}) ions of 2.9 μm median size BAM particles (KEMK63/UF-P1) which were provided by Phosphor Technology Ltd. BAM is widely used in display technology such as plasma display panels [32–34]. It has a β -alumina crystal structure which is made up of spinal blocks, spaced by conduction layers. The BAM:Eu has its barium ions in the conduction layer replaced with Eu^{2+} ions which activate it, producing a highly efficient broad band emission around 450 nm, due to the transition from $4f^6 5d^1$ to $4f^7$ of divalent europium ions [34, 35]. As the temperature increases the emission band broadens and shifts towards the UV. The decay behavior of BAM is governed by activator properties and defects in the crystal structure. Divalent europium shows quite a short decay time in the range of 1 – 10 μs due to the $5d - 4f$ being spin and parity allowed. The decay time for BAM is short, shown to be 1.17 μs at room temperature in [33]. The decay lifetime is a function of temperature and reduces with an increase in temperature. This short lifetime makes BAM an excellent candidate for turbulent flow visualization. It also has a high melting point of approximately 2200 K [36].

It has been reported that the BAM:Eu²⁺ phosphorescence signal starts to degrade when it is heated above a temperature of about 750 K, in an air atmosphere [34, 35]. Both emission and excitation efficiency are affected and studies show that the amount of degradation increases as temperature increases, up to approximately 900 K. Near and above this temperature the emission spectra changes. The blue peak around 450 nm vanishes whilst peaks between 580 and 700 nm, in the red region becomes more prominent, with a maximum around 610 nm. This emission is representative of the trivalent europium ion, consistent with the 4f⁶ intra-configurational transitions [35], which is not considered in this study. It has been shown that when the TP is heated in a non-oxidizing atmosphere, the emission spectrum remains almost unchanged [34]. This evidence points to the degradation mechanism being caused by the divalent europium ion concentration decreasing due to oxidation effects, which results in an increase in trivalent europium ions. There also appears to be a structural variation contributing to the reduced emission around 450 nm, where the location structure of the trivalent ions changes from β -alumina to magnetoplumbite (EuMgAl₁₁O₁₉). The degradation mechanism has been reported only when BAM is heated for long incubation times of greater than 1 hour [34, 35]. Though, it is possible that no degradation effects will occur when BAM experiences an extreme temperature environment for a significantly shorter period of time [21]. The survivability of the BAM signal was proven in [25], where phosphorescence intensity is shown to be the same, prior and subsequent to a combustion event. However, the work in [25] also disregards results above 650 K due to weak signal. The diminishing signal with an increase in temperature is probably due to similar thermal effects as YAG:Dy, such as increased phonon quenching rates at elevated temperatures.

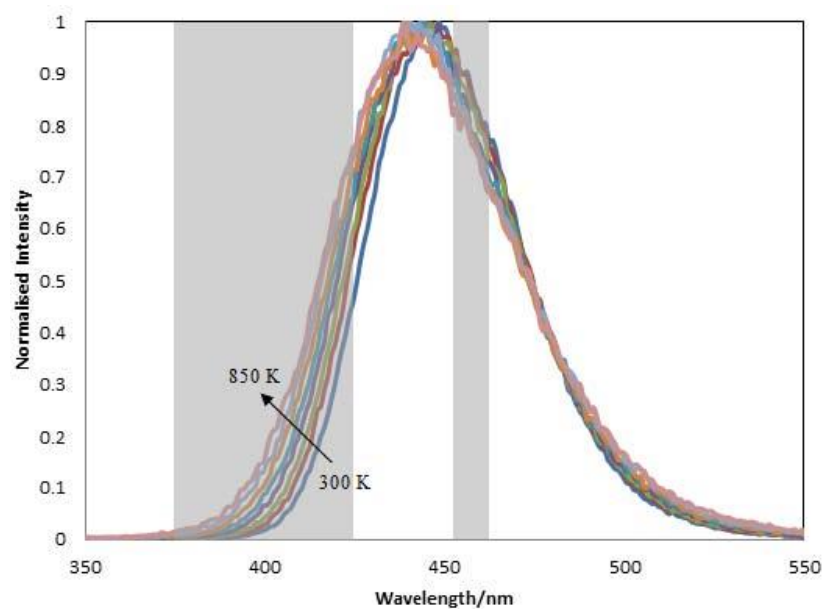


Figure 3. Normalized intensity BAM emission spectra at specified temperatures after 355 nm excitation, determined by surface measurements on a thermocouple coated in BAM using a high

temperature binder, measured in the same position as the jet temperature measurements. The thermocouple was heated in two ways; in the hot air where temperature was varied by varying jet temperature and in a flame where temperature was measured by moving the thermocouple around the flame. The grey areas represent filters placed over the image doubler centered at 400 nm with a FWHM of 50 nm and centered at 458 nm with a FWHM of 10 nm.

2.3 Gas phase thermometry

It is advantageous for gas phase temperature measurements in a flow to use TPs with a short lifetime and shorter camera exposure, in order to keep up with changes that occur with time. This is especially important in turbulent flows where the time resolution must match the characteristic time scales of the flow. Particle size also determines the quality of the results. Tracer particles must be large enough to produce a significant signal, whilst still small enough to follow the flow with sufficient accuracy [37, 38]. The result is a trade-off between the two. Due to size limitations it is feasible to capture the global large scale details of the flow, rather than the small scale details. Gas phase measurements suffer from a relatively low signal, compared with surface measurements [22, 25]. This is due to a low volume density of TPs seeded within the gas. The signal to noise ratio (SNR) can be improved in several ways, including using TPs with a higher signal yield and greater laser fluence. However the laser fluence must not exceed 1.5 J/cm^2 to prevent laser induced heating effects on the TPs [39]. Laser induced breakdown spectroscopy must also be avoided at high laser fluences, which has been documented in [39] and was also experienced in the preliminary phases of this study. Blue emitting phosphors are favorable in high temperature studies as the phosphorescence avoids Planck radiation, providing an improved SNR. TPs with a shorter lifetime can allow for time gating in favor of the phosphorescence signal, discriminating against background signals.

Figures 2 and 3 show experimentally measured phosphorescence signals from YAG:Dy and BAM respectively, depicting how the signals vary with temperature, methodology details are described later. The shaded areas correspond to narrow band filters centered at 458 nm with a FWHM of 10 nm and 492 nm with a FWHM of 10 nm for YAG:Dy and 400 nm with a FWHM of 50 nm and 458 nm with a FWHM of 10 nm for BAM. In order to calculate the temperature using YAG:Dy, the signal intensity of the 458 nm band is divided by that of the 492 nm band. Using BAM, the signal intensity of the 400 nm band is divided by that of the 458 nm band. The filtered spectral areas of each phosphor were chosen via experiment, after careful examination of their respective emission signal, in order to produce the highest temperature sensitivity. The intensity ratio for each phosphor is compared with a previously obtained calibration curve in order to express the local temperature. Optimal gating times were determined experimentally for both phosphors, in order to produce the best SNR, a gatewidth of 100 μs was used for YAG:Dy and a gatewidth of 1 μs was used for BAM. The short gating time which was used with BAM allowed for minimal background disturbances, producing a higher SNR than YAG:Dy.

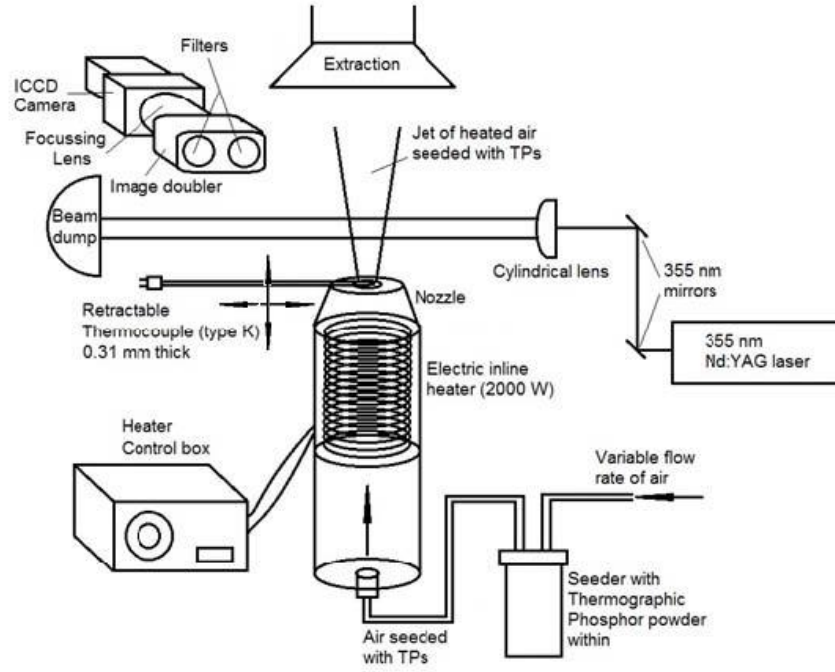


Figure 4. Diagram of experimental setup.

2.4 Flow to particle temperature equilibrium

The TP particles are required to reach thermal equilibrium with the surrounding flow quickly enough to correctly convey the local gas temperature. A recent study has shown via numerical simulation that smaller particles of around 2 μm diameter will adequately respond to a temperature change of 2000 K. However, a larger diameter leads to significantly increased heat capacity, resulting in longer response times and therefore affecting accuracy [21]. The response time can be calculated analytically using the following relationship, refer to [25] for details:

$$t = \frac{\rho_p R_p^2 c_p}{3k_g} \ln \frac{T_p - T_\infty}{T_d - T_\infty} \quad (1)$$

where t is the response time, ρ_p is the density of the TP particle, R_p is its radius, c_p is the specific heat capacity, k_g is the thermal conductivity of the gas, T_p is the temperature of the particle, T_∞ is the gas temperature and T_d is 95% of the gas temperature. The heat capacity of BAM is not known and therefore that of aluminum oxide was used (777 J/kgK) [40], resulting in a response time of 145 μs for 2.6 μm diameter BAM particles, which was deemed adequate to capture the transients of the flow [25].

In this work, the temperature throughout the particle is considered to be homogeneous. This

due to the thermal conductivities of both phosphors being several orders of magnitude higher than the surrounding medium ($k_{BAM} = 24.2 \text{ W/mK}$, $k_{YAG} = 14 \text{ W/mK}$, $k_{air,300 K} = 0.026 \text{ W/mK}$, $k_{air,800 K} = 0.057 \text{ W/mK}$). The same procedure for calculating the response time of the phosphors was used as explained above. The values are set to $k_g = 0.0415 \text{ W/mK}$ (mid way between $k_{air,300 K}$ and $k_{air,800 K}$) with a maximum temperature $T_\infty = 850 \text{ K}$. The densities of

BAM and YAG:Dy are 3700 and 4550 kg/m^3 respectively and the cp of undoped YAG crystal is known to be 590 J/kgK [41]. The cp used for the BAM calculation was also that of aluminum oxide. The response time for the $2.9 \mu\text{m}$ BAM particles was $124 \mu\text{s}$ and the $2.5 \mu\text{m}$ YAG:Dy was $86 \mu\text{s}$, which were deemed acceptable for conveying temperature with sufficient accuracy. The larger $10.2 \mu\text{m}$ YAG:Dy particles showed a 1.4 ms response time which means that they would produce less accurate results.

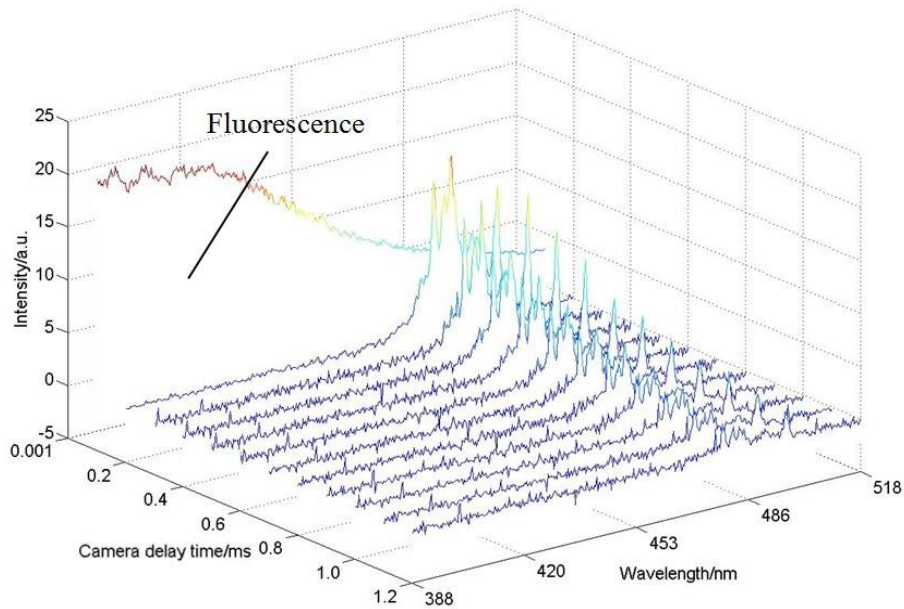


Figure 5. YAG:Dy phosphorescence signal intensity surface measurements at 300 K, taken at different time instances at selected delay increments after successive laser pulses.

3. Experiment

3.1 Heated jet setup

The experimental setup involved feeding standard air through a custom built seeder via a controllable flow rotameter. The thermographic phosphors were seeded using vortex generation and mechanical vibration to disturb the powder, which was subsequently entrained into the flow. The seeded air was heated with a controllable 2000 W inline heater, reaching a maximum temperature of about 850 K. A retractable type K thermocouple was positioned at the exit of the heater in order to

verify the flow temperature. Figure 4 shows a diagram of the entire setup. The thermocouple was removed during phosphor thermometry measurements and replaced immediately after to verify flow temperature.

A free turbulent jet issuing into quiescent air was produced, where the Reynolds number was varied by changing the flow rate or altering the exit nozzle geometry. For time-averaged shots, steep gradient flow restrictors with 2.1, 4.2 and 8.4 mm sized diameters were used to generate turbulent jets, with Reynolds numbers of 10,000, 5,000 and 2,500 respectively. For single shot measurements, the larger 8.4 mm diameter nozzle was used in an attempt to improve resolution and the Reynolds number was varied by changing the airflow rate. Flow rates of 10, 15 and 18 l/min were used, producing Reynolds numbers of 1,650, 2,500 and 3,000 respectively. Increasing the flow rate caused a higher phosphor seeding density within the flow, due to increased turbulence within the seeder. The seeding method produced relatively high density seeding at such low flow rates, compared with commercially available aerosol generators.

The stickiness of the particles has been addressed in previous studies [25, 39]. This property can become a problem in applied optical engine studies where the phosphors can coat the internal surfaces including the optical window and it is shown that using TPs with a transparent, anti-stick coating would reduce the degree of stickiness [25]. The phosphors used herein were uncoated and the smaller 2.5 μm YAG:Dy and 2.9 μm BAM particles tend to stick significantly more than the larger 10.2 μm YAG:Dy particles. This was denoted by the difficulty of seeding of the smaller particles, compared with the larger ones. A higher seeding density could be achieved at lower flow rates using the larger YAG:Dy phosphors.

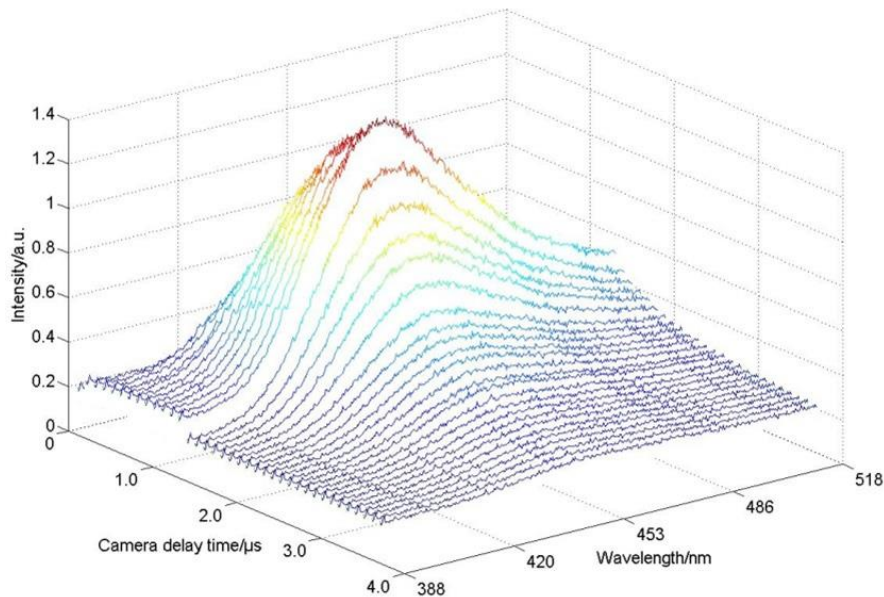


Figure 6. BAM phosphorescence signal intensity surface measurements at 300 K, taken at different time instances at selected delay increments after successive laser pulses.

3.2 Optical setup

Both BAM and YAG:Dy were excited with the third harmonic of a Continuum Surelite II solid state, neodymium doped YAG (Nd:YAG) laser, operated at 10 Hz, using a pulse energy of 20 mJ, for subsequent phosphorescent emission. The laser beam was guided using high reflectivity 355 nm mirrors (99.75% at AOI 45°). Spectral measurements were acquired by focussing the laser beam with a spherical lens and two dimensional measurements were carried out by transforming the beam into a sheet with a cylindrical lens. The laser sheet was 0.5 mm wide and 12 mm high for the accumulated measurements and 0.5 mm wide and 32 mm high for single shot measurements, producing laser fluences of 0.333 and 0.125 J/cm² respectively. Both laser sheets were chopped at the extremities, leaving heights of 10 and 30 mm. The phosphorescence emission was focused by a 50 mm Nikkor lens and collected by an Andor Instaspec V ICCD camera through an image doubler from LaVision. High efficiency filters (>90%), corresponding to the individual TP, were placed over the image doubler. Great care was taken to ensure both parts of the image were the same, through alignment and flat fielding. The camera and laser pulse were synchronized using a Stanford Research DG645 delay generator and were controlled by image acquisition software. Spectra were measured at a maximum of 10 Hz and for 2d spectral filtered images, approximately 7 shots per min were acquired. A short delay had to be incurred due to fluorescence interference after laser excitation, which will be discussed in more detail later. Spectral measurements were taken using an imaging spectrograph, 1/8 m, Oriel MS127i, model 77480, with a single grating of 600 lines/mm, combined with the ICCD camera. The entrance slit width was 50 μm, providing a spectral resolution of less than 1 nm.

It was necessary to correct the phosphorescence images for background interferences prior to processing. This was done using the image acquisition software as part of the acquisition process. Preceding phosphorescence signal acquisition, images of the darkened room were taken, which were then subtracted from the signal on a pixel-by-pixel basis. This would reduce excess noise signals, as well as the dark current produced by the ICCD camera itself. The background corrected images underwent flat fielding using MATLAB to overlay the images for pixel-by-pixel division of the respective emission band intensities. A white light combined with a light box was used to create a uniformly illuminated field for pixel correction. A Gaussian filter of the same size as each image was applied to the images prior to division in order to smooth out fluctuations. Spatial alignment of the images was achieved by capturing a reference image of a grid with symbols, which was positioned in place of the jet. This allowed for exact image mapping in both x and y directions.

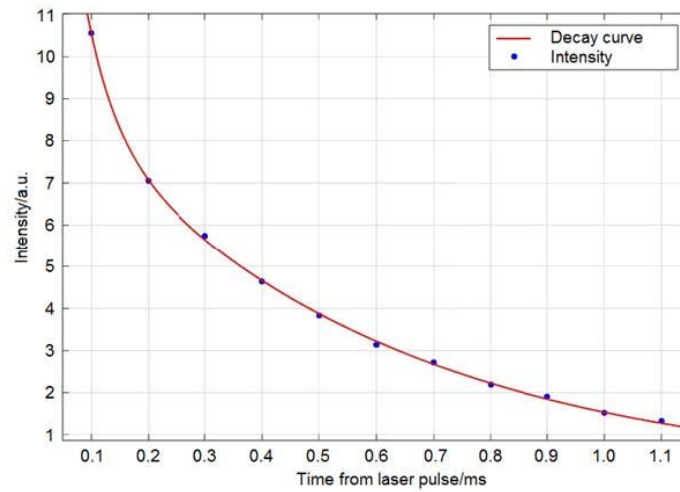


Figure 7. YAG:Dy phosphorescence signal decay curve at room temperature, determined from data points at different time instances from Figure 5 after the point fluorescence vanishes and phosphorescence is detectable, prevailing until the phosphorescence signal reaches the noise level. A double exponential fit was determined in MATLAB.

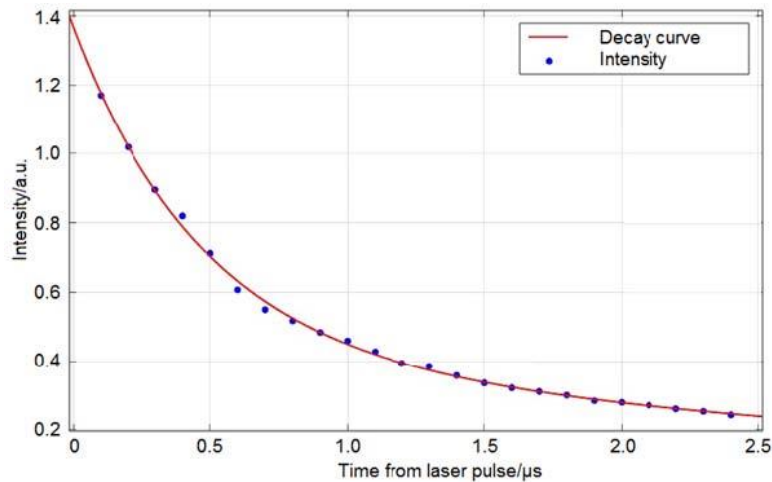


Figure 8. BAM phosphorescence signal decay curve at room temperature, determined from data points at different time instances from Figure 6 after the point fluorescence vanishes and phosphorescence is detectable, prevailing until the phosphorescence signal reaches the noise level. A double exponential fit was determined in MATLAB.

4. Results and discussion

4.1 Calibration

4.1.1 Spectral signal variation with time at 300 K

Both fluorescence and phosphorescence occur as competing de-excitation processes immediately after excitation for BAM and YAG:Dy and both of these emission signals can be seen in Figures 5 and 6. The aforementioned camera gating delay was introduced in order to avoid possible

interference from fluorescence signals, which occur in much shorter timeframes than phosphorescence. Figures 5 and 6 show the entire emission spectra at different time instances, for YAG:Dy and BAM respectively, at selected delay increments of detection after successive laser pulses. The YAG:Dy timescale is in milliseconds, whilst the BAM timescale is in microseconds due to the phosphorescence lifetime variations, allowing Figure 6 to more accurately convey the fluorescence lifetime, compared with Figure 5. The figure shows fluorescence prevailing up to 1 μ s after the laser pulse and therefore this timing was used for the camera gating delay. Phosphorescence emission lifetime reduces with an increase in temperature and no fluorescence signal was present at higher temperatures using these timings and therefore the fluorescence signal lifetime is expected to remain constant or reduce with an increase in temperature. Figures 7 and 8 show the phosphorescence decay lifetime at room temperature, translated from their respective emission histories, beginning after the fluorescence signal disappears, showing YAG:Dy to last for 1.1 ms and BAM approximately 2.5 μ s. Both phosphors have double exponential curves fitted to their respective decay rate which confirmed the observations of [33]. Normally a single exponent is used for temporal method temperature measurements, however in this study the spectral method was used and the nature of the decay signal was not considered. The lifetime of BAM could be different to that shown in [33] due to experimental and methodological differences, such as dopant concentration, TP synthesis procedure, excitation and detection equipment, and detection procedure. In this work the phosphorescence lifetimes were used to determine the optimal camera gating times by comparing the spectral emission intensities measured with the spectrograph at various gatewidths.

4.1.2 Spectral signal variation with temperature

It was essential to carry out the calibration measurements for both phosphors in the same position and with the same optical equipment as the gas phase results, in order to minimise systematic errors which can occur from moving optical equipment [42]. Calibrations were carried out for each TP individually. The calibration procedure involved heating a type K thermocouple with 0.31 mm diameter using two heating methods. The thermocouple was coated with the individual TP using an Omega CC high temperature binder. Care was taken to ensure TP-binder layer of minimal thickness was applied, ensuring that the thermocouple and TP temperature matched as closely as possible. A TP-binder layer thickness of 0.03 mm was measured by taking wire thickness measurements before and after application, using a micrometer.

For temperatures ranging from 300 to 850 K, the hot jet of air produced by the heater was used to heat the thermocouple and for higher temperatures a flame was used to heat the thermocouple from 500 to 1300 K. The thermocouple was moved to different locations within the flame in order to vary its temperature for the calibration measurements. The flame signal had to be subtracted from the phosphorescence signal and this was done in the same way as the background correction in other measurements. The phosphorescence signal was much stronger than the flame incandescence for

surface measurements. The background image in this case was the thermocouple positioned within the flame. A stable, laminar premixed flame was used that remained consistent throughout the measurement process.

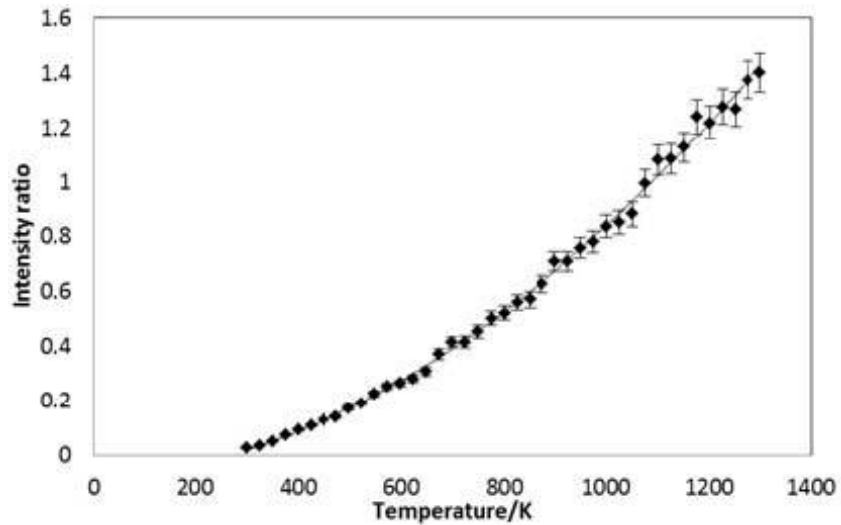


Figure 9. YAG:Dy calibration curve determined from surface measurements of a thermocouple heated to specified set temperatures by dividing the 458 nm filtered emission region by the 492 nm filtered emission region at each temperature.

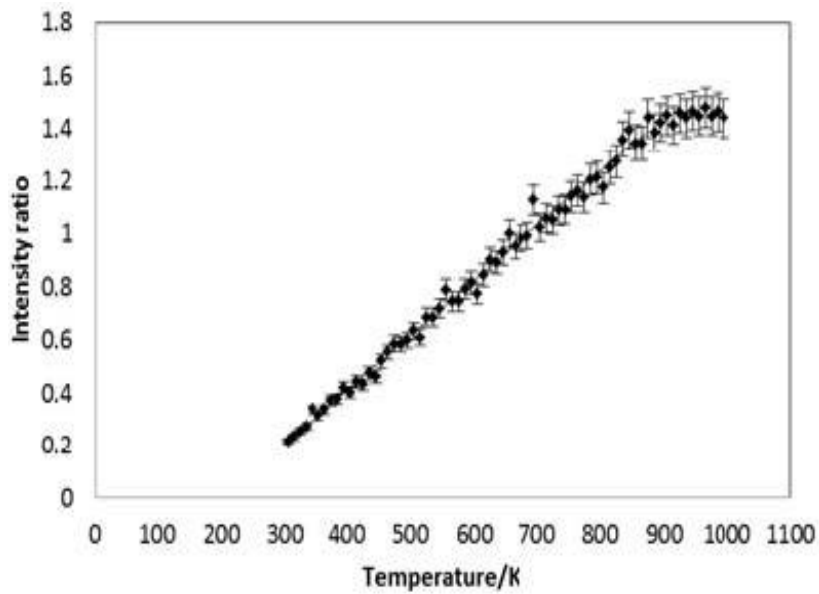


Figure 10. BAM calibration curve determined from surface measurements of a thermocouple heated to specified set temperatures by dividing the 400 nm filtered emission region by the 458 nm filtered emission region at each temperature.

Figures 9 and 10 show the calibration curves for YAG:Dy and BAM respectively, as measured experimentally. The calibration was carried out with and without the spectrograph,

conveying a very similar intensity ratio to temperature relation, with small differences induced by changing the optical equipment. The calibration curves produced for the respective phosphors using both heating methods were almost identical within the overlapping temperature range, revealing that the flame method did not incur any significant errors due to flame incandescence background correction. The phosphorescence emission spectrum was found to be fluence independent within the fluence range tested in this study

4.1.3 Signal intensity variation with temperature

Figure 9 shows the YAG:Dy calibration curve up to 1300 K, where the phosphorescence signal starts to diminish. The upper limit of detection varies from study to study, from 1300 K [31], to almost 1600 K [19, 24], to 1800 K [29], to around 2000 K [27], where the discrepancies could be due to the differences in experimental setup, such as optical equipment and calibration technique. Specifically, in [31] a small particle diameter of 1.8 μm was used, which could have resulted in lower recorded phosphorescence intensity. The work in [19] and [24] uses the same calibration method, involving 4 μm sized particles, using fibres to focus the laser beam and for emission collection, along with an ICCD device coupled with a photomultiplier tube. These factors could all contribute to the high SNR. The study in [29] specifies a doping concentration of 3%, which could be a factor contributing to relatively higher emission, along with the usage of relatively large particle sizes 10 – 100 μm . In [27] the TPs were in powder form, therefore maximum volume density was used. The lifetime method was used with different percentage doping levels, which affected the phosphorescence signal intensity.

The maximum temperature of the heater used here was 850 K and therefore a calibration up to 2000 K was unnecessary. The curve shows an excellent fit, with an R^2 value of 0.9971. The spectral signal strength reduction, with an increase in temperature is shown in Figure 11. This is likely to be the cause of increasing error towards higher temperatures and explains why the data in Figure 2 appear noisier at elevated temperatures. The emission characteristics for both YAG:Dy particle sizes were identical for surface measurements.

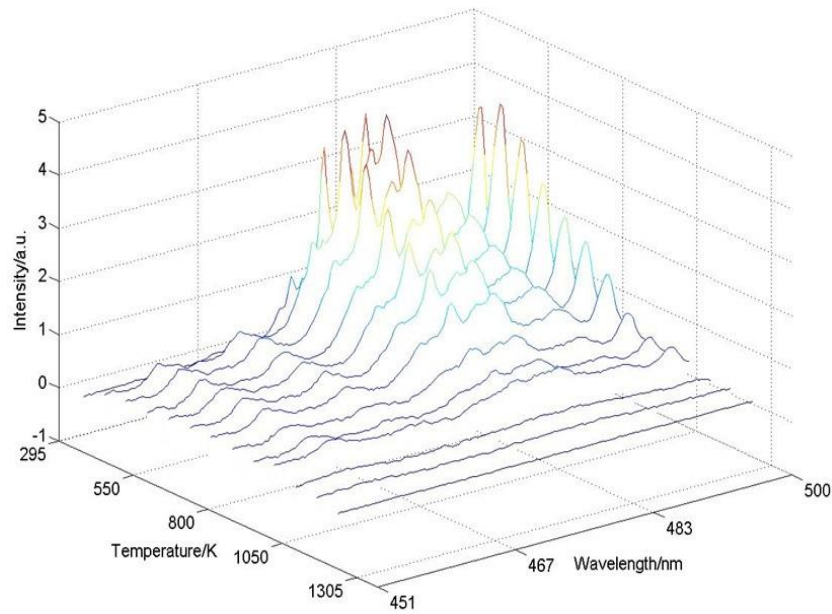


Figure 11. YAG:Dy spectral intensity variation with change in temperature determined from surface measurements of a thermocouple heated to specified set temperatures.

Figure 10 shows the BAM calibration curve up to 1000 K. The intensity ratio became insensitive to temperature change near 875 K, where the calibration curve began to flatten, reaching a maximum point. A curve was fitted to the linear part of the data, with a good fit, displaying an R^2 value of 0.9924. Other studies show temperature dependence up to 650 -700 K [21, 25] and 1150 K [39] where again, inconsistencies could be due to experimental setup. Specifically, the study in [21] does not investigate temperatures above 700 K and in [25] a relatively low laser fluence of 0.04 J/cm^2 was used and the phosphorescence emission intensity depends on the excitation energy, which could be why phosphorescence was only detected up 650 K. The work in [39] uses a longer exposure time of $8 \text{ } \mu\text{s}$, along with larger particles of $4.2 \text{ } \mu\text{m}$ diameter and significantly higher laser fluences up to 1.5 J/cm^2 , which can all lead to producing a higher SNR, possibly revealing a phosphorescence emission up to higher temperatures than recorded herein.

The temperature dependence range exceeds that of the maximum temperature of the heater and therefore is sufficient in this case. Figure 12 depicts the spectral signal strength reduction, with increasing temperature, showing that the phosphorescence signal vanishes around 1100 K. This signal reduction may account for the larger error at high temperatures. These results, along with other studies [21, 25, 39] show that despite its high melting point, BAM shows a weakened signal at elevated temperatures and therefore may not be suitable for high temperature combustion measurements.

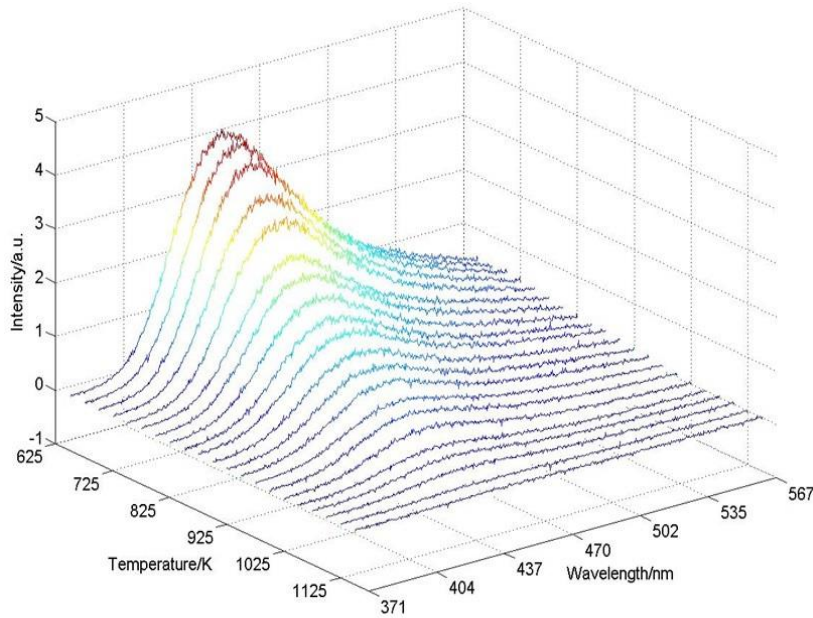


Figure 12. BAM spectral intensity variation with change in temperature determined from surface measurements of a thermocouple heated to specified set temperatures.

4.2 Jet temperature distributions

4.2.1 Single shot results using BAM

The 2.9 μm BAM particles produced a strong signal when seeded within the gas flow, which allowed for detailed single shot measurements to be made at various temperatures ranging from 500 – 850 K. Single shot measurements with BAM in heated jets were also achieved in

[21] up to 700 K. Herein, thermometry measurements were taken at heater temperature settings of 500, 600, 700 and 850 K. At each temperature and each position above the nozzle 50 background images and 50 phosphorescence images were taken and the average background signal was used for background correction. The laser sheet was 30 mm high and images were taken at various heights above the nozzle, covering a large portion of the jet, with a maximum height of 90 mm. The jet was kept at constant temperature throughout each set of measurements, verified by the thermocouple.

Figure 13 shows single shot phosphorescence intensity images of a jet at 850 K, filtered at the 458 nm (left) and 400 nm (right) emission bands. It can be seen that the phosphorescence signal is greater towards the middle of the jet, gradually reducing with radial distance, due to seeding density. Other studies based on heated jets produced similar results [21, 22]. The low signal towards the edges of the jet necessitated the use of conditional threshold filtering, which was applied to image intensities below a certain value, in order to prevent intensity ratio calculations in regions where there was little or no signal present. These regions would produce high noise and therefore inaccurate

data due to the low SNR. This feature was also seen in [22].

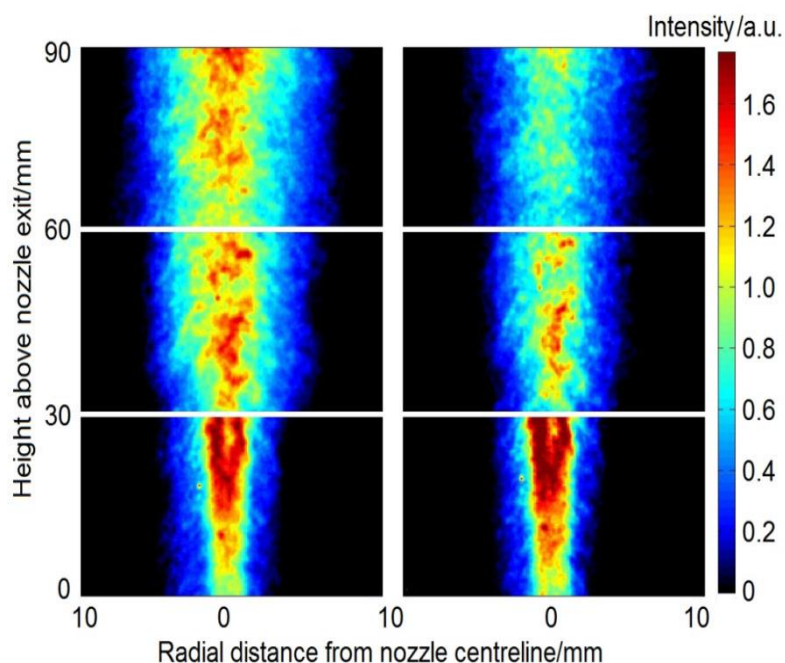


Figure 13. Gas phase single shot BAM phosphorescence emission intensity images of the 458 nm region (left) and the 400 nm region (right) from a jet at 850 K, where temperature was confirmed by a thermocouple inserted near the nozzle and centrally in the flow before and after measurements.

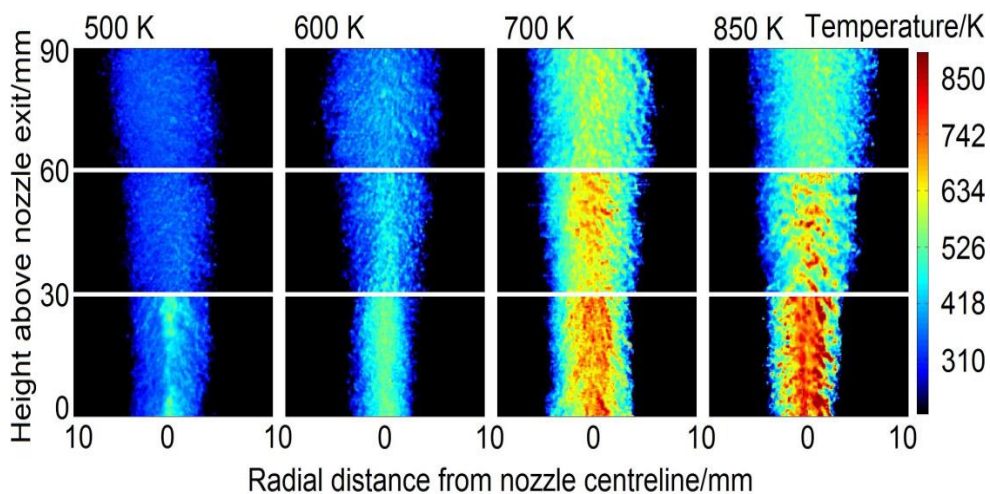


Figure 14. Gas phase single shot temperature distributions of jets with a Reynolds number of 2500 (8 mm diameter), conveyed with BAM phosphorescence, using the intensity ratio method by carrying out pixel to pixel divisions of the 400 nm region by the 458 nm region.

Figure 14 shows the stacked temperature distributions, conveying BAM phosphorescence emission ratio for jets at the specified set temperatures, with a Reynolds number of 2,500. The

temperature does not exactly match up in corresponding stacked images due to the turbulent nature of the jets, different time instances of the image acquisition process and variations in the flow at a given experimental condition. The high signal yield produced by BAM at such short lifetimes and hence, short camera gating times, allows for shear layers be identified in each jet, along with the spatial temperature profile. Similar features can be seen in the results of [21, 22]. The temperature is higher in the central part of the jets, gradually dissipating radially outwards and upwards from the nozzle exit. The temperature profiles determined in this study match those found in the literature, for example [21, 43, 44].

4.2.2 Time averaged results using BAM

Figure 15(a) shows the phosphorescence images acquired at 458 nm (left) and 400 nm (right) for a 300 K jet at $Re = 5000$ and Figure 15(b) shows the corresponding jet temperature distribution. It can be seen that the lower temperature jets appear smaller in diameter when compared with the equivalent jets at higher temperature. This is because the BAM phosphorescence signal intensity in the 400 nm region is much lower than that of the 458 nm region, which results in a low intensity ratio, conveying a temperature close to the temperature scale minimum. This effect is minimized for images with an intensity ratio of 1. Another observation from Figure 15(b) shows that despite the phosphorescence signal inhomogeneity, the phosphorescence intensity ratio for the jet at 300 K is still relatively homogeneous. This result is supported by the work presented in [42].

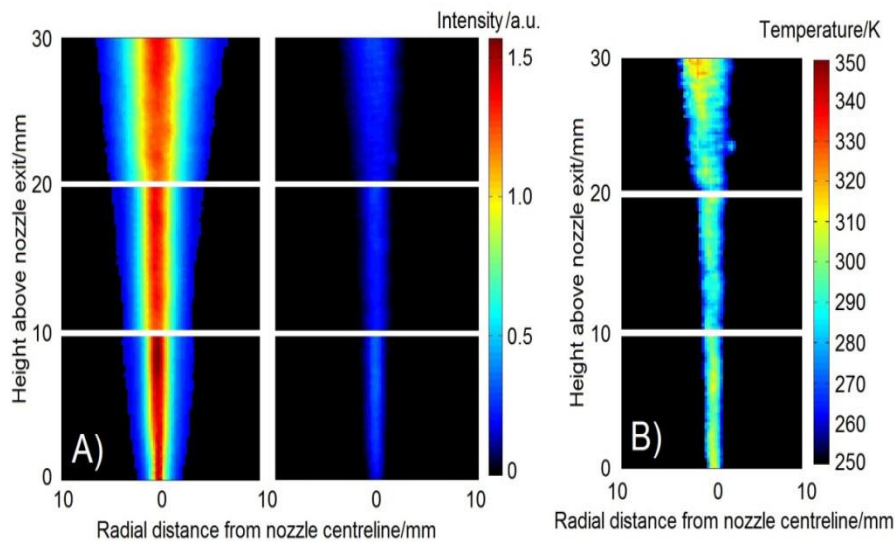


Figure 15. (a) Gas phase time averaged phosphorescence intensity images of the 458 nm band (left) and the 400 nm band (right) from the BAM phosphorescence emission at 300 K with a Reynolds number of 5,000. (b) 100 shot time averaged intensity ratio image found by carrying out pixel to pixel divisions of the 400 nm region by the 458 nm region of (a).

The time averaged temperature distributions produced by BAM at near nozzle positions of jets at various temperatures from 300 to 700 K at different Reynolds numbers are presented in Figure 16, where the Reynolds number was varied by changing the diameter of the nozzle exit. Thermometry measurements were taken at heater temperature settings of 300, 500, 600 and 700 K, for the three Reynolds numbers investigated. At each temperature and each position above the nozzle 100 background images and 100 phosphorescence images were taken. The laser sheet was 10 mm high and the images were taken up to 30 mm height above the nozzle exit, presented as stacked images. The jet temperatures throughout each set of measurements were verified by the thermocouple. The temperature profiles match up in corresponding stacked images, despite turbulence, due to the results being time averaged. The flow pattern cannot be identified in the time averaged data, however the spatial temperature profiles are more prominent compared with the single shot results. These features are also seen in the time averaged results in [21, 22]. The flow appears to diverge more at higher Reynolds number.

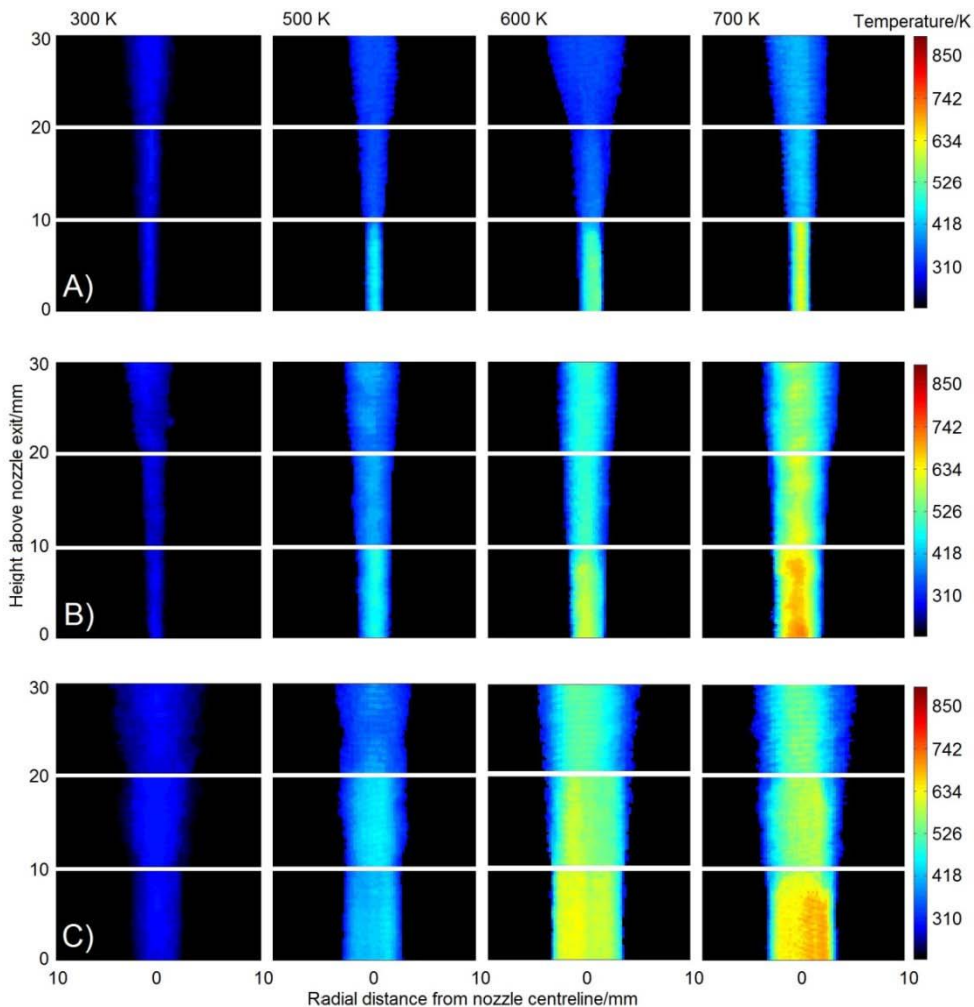


Figure 16. Gas phase 100 shot time averaged temperature distributions for various temperatures and Reynolds numbers, conveyed with BAM phosphorescence, using the intensity ratio method by carrying out pixel to pixel divisions of the 400 nm region by the 458 nm region. (a) shows jets with a Reynolds number of 10,000 achieved using a nozzle diameter of 2 mm (b) shows jets with a

Reynolds number of 5,000 achieved using a nozzle diameter of 4 mm and (c) shows jets with a Reynolds number of 2,500 achieved using a nozzle diameter of 8 mm.

4.2.3 Single shot and time averaged results using YAG:Dy

There was a very negligible amount of the phosphorescence signal produced by the 2.5 μm diameter YAG:Dy particles when seeded within the flow. This can be explained by the excitation and emission characteristics of the YAG:Dy phosphor becoming more transparent to visible light as it increases in size, reducing trapping efficiency caused by light scattering of particles [38]. Therefore at smaller sizes less luminescence is produced. This, combined with a relatively low seeding density, compared with surface measurements, resulted in little or no measured emission of phosphorescence for the jets both for single shot and time averaged measurements. This low signal effect was also mentioned in [25] where the authors mitigated the usage of BAM instead of YAG:Dy, in order to produce gas phase results.

The 10.2 μm YAG:Dy did produce relatively better phosphorescence signal than the 2.5 μm YAG:Dy particles, but still there was not a high enough phosphorescence signal yield for single shot measurements. However, accumulating a number of single shot images resulted in an average temperature distribution. It has also been documented in [23] that the SNR of YAG:Dy is low, where the principle of superpixels is necessitated. Superpixels combine the intensities in regions consisting of multiple pixels, for example using 5x5 pixels to improve SNR. However, in this study it was sufficient to accumulate the data for an improved SNR. It was also beneficial not to use superpixels here, in the interest of comparing the results of the two phosphors, as well as preserving the spatial resolution of the images.

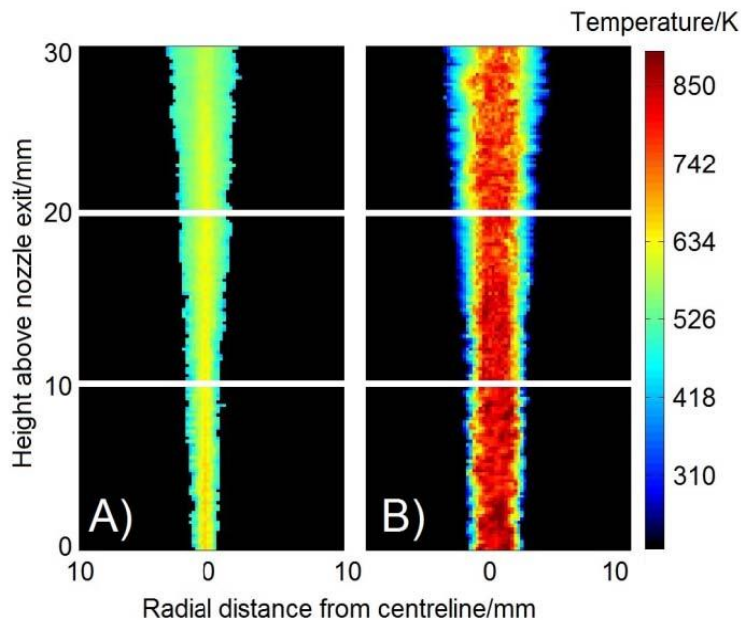


Figure 17. Gas phase 100 shot, time-averaged temperature distributions conveyed with YAG:Dy phosphorescence, using the intensity ratio method by carrying out pixel to pixel divisions of the 458 nm region by the 492 nm region for (A) A jet at 600 K with a Reynolds number of 5,000 achieved with a nozzle diameter of 4 mm and (B) a jet at 850 K with a Reynolds number of 2,500 achieved with a nozzle diameter of 8 mm.

The 458 nm emission band of the YAG:Dy conveyed no appreciable signal near room temperature and at low temperatures up to about 500 K, during gas phase measurements. This, combined with the application of conditional threshold filtering, mentioned above, meant that jets at temperatures below 550 K could not be accurately deduced using YAG:Dy. Figure 17 shows temperature distributions for two jets, where each image was an average of 100 shots. It can be seen from the less pronounced jet temperatures, that the signal strength is less than that of the BAM time-averaged shots. The figure shows a jet at 600 K with a Reynolds number of 5,000 (left) and a jet at 850 K with a Reynolds number of 2,500 (right). In order to get a good SNR at 600 K, the seeding density had to be increased and therefore a nozzle diameter of 4 mm was used, instead of 8 mm. This was done in order to increase the signal yield of the 458 nm band. Only two jets of temperatures of 600 K and 850 K are presented using YAG:Dy. In Figures 17(a) and 17(b) the jets appear thinner relative to the corresponding BAM measurements of jets taken at the same temperature and Reynolds number. This is again due to a low phosphorescence signal produced at low temperatures in the 458 nm region, for YAG:Dy, producing a low intensity ratio and hence conveying a temperature close to the temperature scale minimum. The YAG:Dy calibration curve in Figure 9 is steeper towards higher temperatures and the jet temperature distributions show only a small change over a variation of 250 K. This shows that YAG:Dy displays less sensitivity to temperature change, compared with BAM at this range.

4.2.4 Precision and uncertainty

The precision of the gas phase LIP thermometry technique was calculated using single shot BAM phosphorescence images from the near nozzle part of the gas jets, within the central region. Five matching pixels were compared from each of the 50 single shot images at every temperature increment presented in the results. Figure 18 depicts the number of pixels conveying specific temperatures for each temperature set. The standard deviation of the results at 300 K was 8.6 K (2.8%), increasing up to 49.8 K (5.9%) at 850 K, showing a decrease in precision and increase in uncertainty with an increase in temperature. The data for each temperature was corrected using conditional filtering in such a way that the temperature did not go below 280 K. The YAG:Dy phosphor could not be used for this analysis as its emission signal was not strong enough for single shot analysis. However there is expected to be a further inaccuracy induced when using the YAG:Dy due to the larger diameter and hence longer response times with change in temperature. This, combined with having to average data shows that YAG:Dy is more suited to steadier situations, such

as laminar jets with low temperature and velocity gradients.

The amount of error induced by the thermocouple gas temperature measurement was approximately ± 0.2 K at 300 K and about ± 4.3 K at 850 K. The heater induced an error of up to ± 5 K for temperatures below about 550 K, increasing to between 10 and 15 K at 850 K. The data is expected to convey a bias towards higher temperature as only the hot jet flow is seeded and therefore cooler entrained air is only represented by the amount the hot jet is cooled.

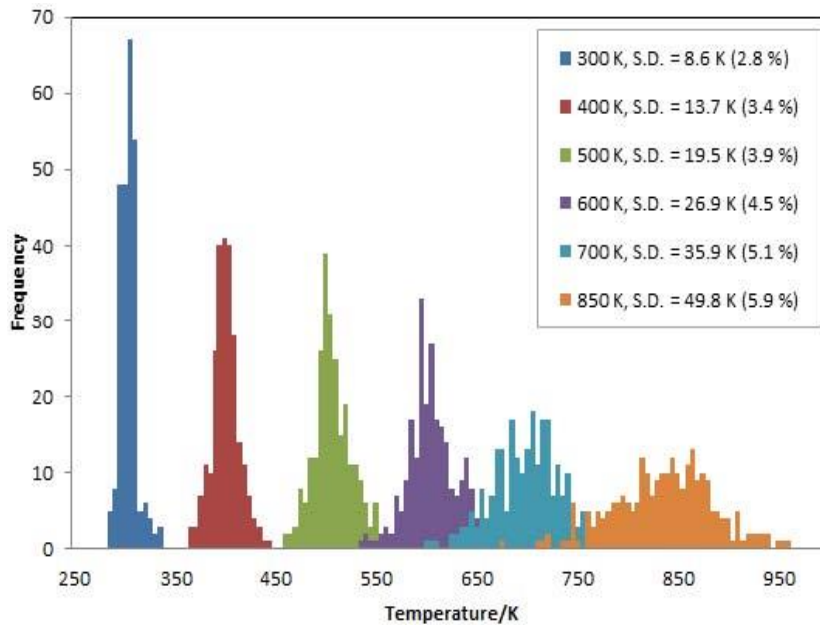


Figure 18. Histograms of gas phase LIP temperature measurements from 5 matching pixels in the same region of 50 individual BAM single shot images at each temperature used in this study.

Time averaged thermocouple data was compared against the time averaged temperature distribution from the BAM and YAG:Dy phosphorescence data to find the error induced by each individual phosphor. A thermocouple was placed at specific heights above the nozzle, centrally in the jet and pixels matching these areas in BAM and YAG:Dy time averaged temperature images were compared to the thermocouple measurements. The difference in temperature at each position was calculated and converted to a percentage of the thermocouple temperature reading. The analysis revealed that there was an error of up to 3.1% for BAM, taken as an average over all of the positions measured. For YAG:Dy, the error increased as the height above nozzle increased, from 4.4% at 5 mm above the nozzle exit, up to 10.1% at 25 mm above the nozzle. It is possible that the greater error is because the larger diameter particles of YAG:Dy retain their heat for longer.

5. Conclusion

Planar laser induced phosphorescence was used in conjunction with thermographic phosphors BAM and YAG:Dy to determine the temperature distribution of heated jets with different Reynolds numbers and at a range of temperatures. YAG:Dy conveyed no appreciable phosphorescence signal at 2.5 μm diameter when seeded within the gas flow, however larger

10.2 μm YAG:Dy particles did produce a high enough signal for gas phase temperature measurements. The 2.9 μm BAM particles produced a higher phosphorescence signal yield, compared with both 2.5 and 10.2 μm YAG:Dy particle diameters, therefore single shot results with high SNR were acquired using BAM, but not with YAG:Dy. Both phosphors could be used to express time averaged temperature distributions, due to an increase in signal to noise ratio that could be achieved by accumulating images.

The YAG:Dy and BAM phosphorescence signal strengths are shown to decrease with an increase in temperature and diminish around 1300 K and 1100 K respectively, where BAM only shows temperature sensitivity up to 875 K. The phosphorescence lifetimes at room temperature are shown to be approximately 1.1 ms for YAG:Dy and 2.5 μs for BAM.

The high emission intensity produced by BAM allowed for detailed jet temperature distributions to be made at various temperatures up to 850 K, displaying a large portion of the jet, up to 90 mm above the nozzle exit. The fact that BAM phosphorescence emission intensity is high at short gating times of around 1 μs means that it is capable of detecting the flow structure at this characteristic time scale in the jet. Raw images at 300 K show the intensity ratio is almost homogeneous despite phosphorescence signal inhomogeneity. Near nozzle time averaged images were produced for both of the phosphors, where the spatial temperature distributions are clearly defined and the characteristics of different jets were identified.

The precision and uncertainty of the experiment were investigated, where the standard deviation of the results at 300 K was 8.6 K (2.8%), increasing up to 49.8 K (5.9%) at 850 K, showing a decrease in precision and increase in uncertainty with an increase in temperature. The largest calculated error for BAM was 3.1% and for YAG:Dy 10.1%, where the discrepancy is likely to be due to the larger sized YAG:Dy particles and hence, longer response times. BAM is suitable for turbulent flow situations, whereas YAG:Dy displays less sensitivity within the temperature range in this study and a slower response time to temperature changes.

References and links

1. W. M. Yen, S. Shionoya, and H. Yamamoto, *Phosphor Handbook*, 2nd Ed. (CRC Press/Taylor and Francis, 2007).
2. S. W. Allison and G. T. Gilles, "Remote thermometry with thermographic phosphors: instrumentation and applications," *Rev. Sci. Instrum.* 68(7), 2615–2650 (1997).
3. N. J. Turro, J. C. Scaiano, and V. Ramamurthy, *Principles of Molecular Photochemistry: an*

Introduction (University science books, 2009).

4. M. Aldén, A. Omrane, M. Richter, and G. Sarner, "Thermographic phosphors for thermometry: a survey of combustion applications," *Prog. Energ. Combust.* 37(4), 422–461 (2011).
5. N. Fuhrmann, J. Brubach, and A. Dreizler, "Phosphor thermometry: a comparison of the luminescence lifetime and the intensity ratio approach," *Proc. Combust. Inst.* 34(2), 3611–3618 (2013).
6. S. A. Wade, S. F. Collins, and G. W. Baxter, "Fluorescence intensity ratio technique for optical fiber point temperature sensing," *J. Appl. Phys.* 94(8), 4743–4756 (2003).
7. S. Someya, S. Yoshida, Y. Li, and K. Okamoto, "Combined measurement of velocity and temperature distributions in oil based on the luminescent lifetimes of seeded particles," *Meas. Sci. Technol.* 20(2), 025403 (2009).
8. A. Omrane, F. Ossler, M. Alden, U. Gtoransson, and G. Holmstedt, "Surface temperature measurement of flame spread using thermographic phosphors," *Fire Safety Science* 7, 141–152 (2003).
9. G. Särner, M. Richter, and M. Aldén, "Two-dimensional thermometry using temperature-induced line shifts of ZnO:Zn and ZnO:Ga fluorescence," *Opt. Lett.* 33(12), 1327–1329 (2008).
10. J. I. Eldridge, T. J. Bencic, S. W. Allison, and D. L. Beshears, "Depth-penetrating temperature measurements of thermal barrier coatings incorporating thermographic phosphors," *J. Therm. Spray Technol.* 13(1), 44–50 (2004).
11. N. Fuhrmann, M. Schild, D. Bensing, S. A. Kaiser, C. Schulz, J. Brubach, and A. Dreizler, "Two-dimensional cycle-resolved exhaust valve temperature measurements in an optically accessible internal combustion engine using thermographic phosphors," *Appl. Phys. B* 106(4), 945–951 (2012).
12. K. W. Tobin, S. W. Allison, M. R. Cates, G. J. Capps, and D. L. Beshears, "High temperature phosphor thermometry of rotating turbine blades," *AAIA J.* 28(8), 1485–1490 (1990).
13. B. W. Noel, H. M. Borella, W. Lewis, W. D. Turley, D. L. Beshears, G. J. Capps, M. R. Cates, J. D. Muhs, and K. W. Tobin, "Evaluating thermographic phosphors in an operating turbine engine," *J. Eng. Gas Turbines Power* 113(2), 242–245 (1991).
14. J. P. Feist, A. L. Heyes, and S. Seedfelt, "Thermographic phosphors for gas turbine instrumentation development and measurement uncertainties," *Proceedings of the 11th International Symposium on Applications of Laser Techniques to Fluid Mechanics*, p. 18 (2002).
15. J. Brubach, C. Pflitsch, A. Dreizler, and B. Atakan, "On surface temperature measurements with thermographic phosphors: a review," *Prog. Energ. Combust.* 39(1), 37–60 (2013).
16. A. Omrane, G. Juhlin, F. Ossler, and M. Aldén, "Temperature measurements of single droplets by use of laser-induced phosphorescence," *Appl. Opt.* 43(17), 3523–3529 (2004).
17. A. Omrane, G. Sarner, and M. Aldén, "2D-temperature imaging of single droplets and sprays using thermographic phosphors," *Appl. Phys. B* 79(4), 431–434 (2004).
18. J. Brubach, A. Patt, and A. Dreizler, "Spray thermometry using thermographic phosphors," *Appl. Phys. B* 83(4), 499–502 (2006).
19. R. Hasegawa, I. Sakata, H. Yanagihara, B. Johansson, A. Omrane, and M. Aldén,

- “Two-dimensional gas-phase temperature measurements using phosphor thermometry,” *Appl. Phys. B* 88(2), 291–296 (2007).
20. A. Omrane, P. Petersson, M. Aldén, and M. A. Linne, “Simultaneous 2D flow velocity and gas temperature measurements using thermographic phosphors,” *Appl. Phys. B* 92(1), 99–102 (2008).
21. B. Fond, C. Abram, A. L. Heyes, A. M. Kempf, and F. Beyrau, “Simultaneous temperature, mixture fraction and velocity imaging in turbulent flows using thermographic phosphor tracer particles,” *Opt. Express* 20(20), 22118–22133 (2012).
22. D. A. Rothamer and J. Jordan, “Planar imaging thermometry in gaseous flows using upconversion excitation of thermographic phosphors,” *Appl. Phys. B* 106(2), 435–444 (2012).
23. G. Jovicic, L. Zigan, S. Pfadler, and A. Leipertz, “Simultaneous two-dimensional temperature and velocity measurements in a gas flow applying thermographic phosphors,” in *16th International Symposium on Applications of Laser Techniques to Fluid Mechanics*, Lisbon, Portugal (2012).
24. R. Hasegawa, I. Sakata, H. Yanagihara, G. Sarnier, M. Richter, M. Aldén and B. Johansson, “Two-dimensional temperature measurements in engine combustion using phosphor thermometry,” *SAE J.-Automot. Eng. Paper number 2007-01-1883*, 1797-1803 (2007).
25. P. J. van Lipzig, M. Yu, N. J. Dam, C. C. M. Luijten and L. P. H. de Goey, “Gas phase thermometry in a high pressure cell using BaMgAl₁₀O₁₇:Eu as a thermographic phosphor,” submitted to *Appl. Phys. B* (in revision) (2012).
26. G. S. R. Raju, H. C. Jung, J. Y. Park, J. W. Chung, B. K. Moon, J. H. Jeong, S.-M. Son, and J. H. Kim, “Sintering temperature effect and luminescent properties of Dy³⁺:YAG nanophosphor,” *J. Optoelectron. Adv. Mater.* 12(6), 1273–1278 (2010).
27. M. R. Cates, S. W. Allison, S. L. Jaiswal, and D. L. Beshears, “YAG:Dy and YAG:Tm fluorescence to 1700 C,” in *49th International Instrumentation Symposium*, Orlando, Florida (2003).
28. S. J. Skinner, J. P. Feist, I. J. E. Brooks, S. Seefeldt, and A. L. Heyes, “YAG:YSZ composites as potential thermographic phosphors for high temperature sensor applications,” *Sensor. Actuat. Biol. Chem.* 136, 52–59 (2009).
29. L. P. Goss, A. A. Smith, and M. E. Post, “Surface thermometry by laser-induced fluorescence,” *Rev. Sci. Instrum.* 60(12), 3702–3706 (1989).
30. J. L. Caslavsky and D. J. Viechnicki, “Melting behaviour and metastability of yttrium aluminium garnet (YAG) and YAlO₃ determined by optical differential thermal analysis,” *J. Mater. Sci.* 15(7), 1709–1718 (1980).
31. M. Yu, G. Sarnier, C. C. M. Luijten, M. Richter, M. Aldén, R. S. G. Baert, and L. P. H. de Goey, “Survivability of thermographic phosphors (YAG:Dy) in a combustion environment,” *Meas. Sci. Technol.* 21(3), 037002 (2010).
32. C. R. Ronda, “Recent achievements in research on phosphors for lamps and displays,” *J. Lumin.* 72-74, 49–54 (1997).
33. T. Justel, H. Bechtel, W. Mayr, and D. U. Wiechert, “Blue emitting BaMgAl₁₀O₁₇:Eu with a blue body color,” *J. Lumin.* 104(1-2), 137–143 (2003).
34. K.-B. Kim, K.-W. Koo, T.-Y. Cho, and H.-G. Chun, “Effect of heat treatment on photoluminescence behaviour of BaMgAl₁₀O₁₇:Eu phosphors,” *Mater. Chem. Phys.* 80(3), 682–689 (2003).

35. G. Bizarri and B. Moine, "On BaMgAl₁₀O₁₇:Eu²⁺ phosphor degradation mechanism: thermal treatment effects," *J. Lumin.* 113(3-4), 199–213 (2005).
36. D. Ravichandran, R. Roy, W. B. E. S. White, and S. Erdei, "Synthesis and characterisation of sol-gel derived hexa-aluminate phosphors," *J. Mater. Res.* 12(3), 819–824 (1997).
37. A. Melling, "Tracer particles and seeding for particle image velocimetry," *Meas. Sci. Technol.* 8(12), 1406–1416 (1997).
38. N. T. Tran, J. P. You, and F. G. Shi, "Effect of phosphor particle size on luminous efficacy of phosphor-converted white LED," *J. Lightwave Technol.* 27(22), 5145–5150 (2009).
39. J. Lindén, N. Takada, B. Johansson, M. Richter, and M. Aldén, "Investigation of potential laser-induced heating effects when using thermographic phosphors for gas-phase thermometry," *Appl. Phys. B* 96(2-3), 237–240 (2009).
40. D. C. Ginnings and G. T. Furukawa, "Heat capacity standards for the range 14 to 1200 K," *J. Am. Chem. Soc.* 75(3), 522–527 (1953).
41. W. Koechner, *Solid-State Laser Engineering, 6th Edition* (Springer science and business media inc., 2006).
42. J. Lindén, C. Knappe, M. Richter, and M. Aldén, "Precision in 2D temperature measurements using the thermographic phosphor BAM," *Meas. Sci. Technol.* 23(8), 085205 (2012).
43. F. Lemoine, Y. Antoine, M. Wolff, and M. Lebouche, "Simultaneous temperature and 2D velocity measurements in a turbulent heated jet using combined laser-induced fluorescence and LDA," *Exp. Fluids* 26(4), 315–323 (1999).
44. A. Agrawal, K. R. Sreenivas, and A. K. Prasad, "Velocity and temperature measurements in an axisymmetric turbulent jet with cloud-like off-source heating," *Int. J. Heat Mass Tran.* 47(6-7), 1433–1444 (2004).

Acknowledgments

The authors would like to thank the Thomas Gerald Gray Charitable Trust for the PhD studentship and making the project possible, along with Phosphor Technology for their contribution and the technicians Kenneth Anstiss, Costas Xanthos, Clive Barret and Andrew Selaway for their efforts and guidance towards equipment setup.